

## Accepted Manuscript

A combined EPR and MD simulation study of a nitroxyl spin label with restricted internal mobility sensitive to protein dynamics.

Vasily S. Oganessian, Fatima Chami, Gaye F. White, Andrew J. Thomson

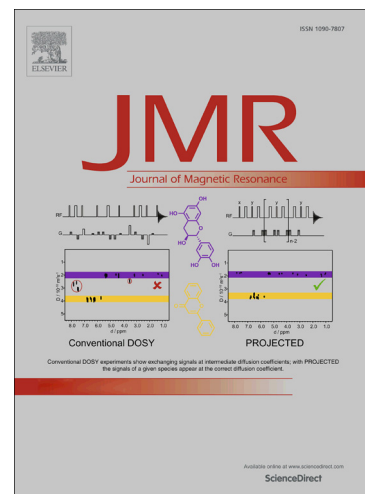
PII: S1090-7807(16)30227-0  
DOI: <http://dx.doi.org/10.1016/j.jmr.2016.11.001>  
Reference: YJMRE 5981

To appear in: *Journal of Magnetic Resonance*

Received Date: 26 August 2016  
Revised Date: 31 October 2016  
Accepted Date: 1 November 2016

Please cite this article as: V.S. Oganessian, F. Chami, G.F. White, A.J. Thomson, A combined EPR and MD simulation study of a nitroxyl spin label with restricted internal mobility sensitive to protein dynamics., *Journal of Magnetic Resonance* (2016), doi: <http://dx.doi.org/10.1016/j.jmr.2016.11.001>

This is a PDF file of an unedited manuscript that has been accepted for publication. As a service to our customers we are providing this early version of the manuscript. The manuscript will undergo copyediting, typesetting, and review of the resulting proof before it is published in its final form. Please note that during the production process errors may be discovered which could affect the content, and all legal disclaimers that apply to the journal pertain.



**A combined EPR and MD simulation study of a nitroxyl  
spin label with restricted internal mobility sensitive to  
protein dynamics.**

*Vasily S. Oganesyan\*, Fatima Chami, Gaye F. White and Andrew J. Thomson*

*School of Chemistry, University of East Anglia, Norwich, NR4 7TJ,*

*United Kingdom*

\*Corresponding author: E-mail: [v.oganesyan@uea.ac.uk](mailto:v.oganesyan@uea.ac.uk)

**A combined EPR and MD simulation study of a nitroxyl spin  
label with restricted internal mobility sensitive to protein  
dynamics.**

*Vasily S. Oganessian, Fatima Chami, Gaye F. White, Andrew J. Thomson*

**Abstract**

EPR studies combined with fully atomistic Molecular Dynamics (MD) simulations and an MD-EPR simulation method provide evidence for intrinsic low rotameric mobility of a nitroxyl spin label, Rn, compared to the more widely employed label MTSL (R1). Both experimental and modelling results using two structurally different sites of attachment to Myoglobin show that the EPR spectra of Rn are more sensitive to the local protein environment than that of MTSL. This study reveals the potential of using the Rn spin label as a reporter of protein motions.

**Introduction**

Nitroxide spin probes covalently bound at selected sites on proteins provide a useful tool for the study of protein motions, both global and local, using continuous wave (CW) EPR spectroscopy (1-8). The widely used spin label (MTSL), containing a nitroxide radical, is linked via a disulphide bond to the sulfur of a cysteine residue forming a four atom side-chain, denoted R1 (1-5, 9, 10). Although the inherent flexibility of R1, arising from five dihedral angles (Figure 1), allows the introduction of this spin label (SL) to many accessible sites of a protein it does not allow the unambiguous separation of side-chain motional

dynamics from that of the protein.(9-14) In fact, the rich conformational dynamics of the MTSL label and its

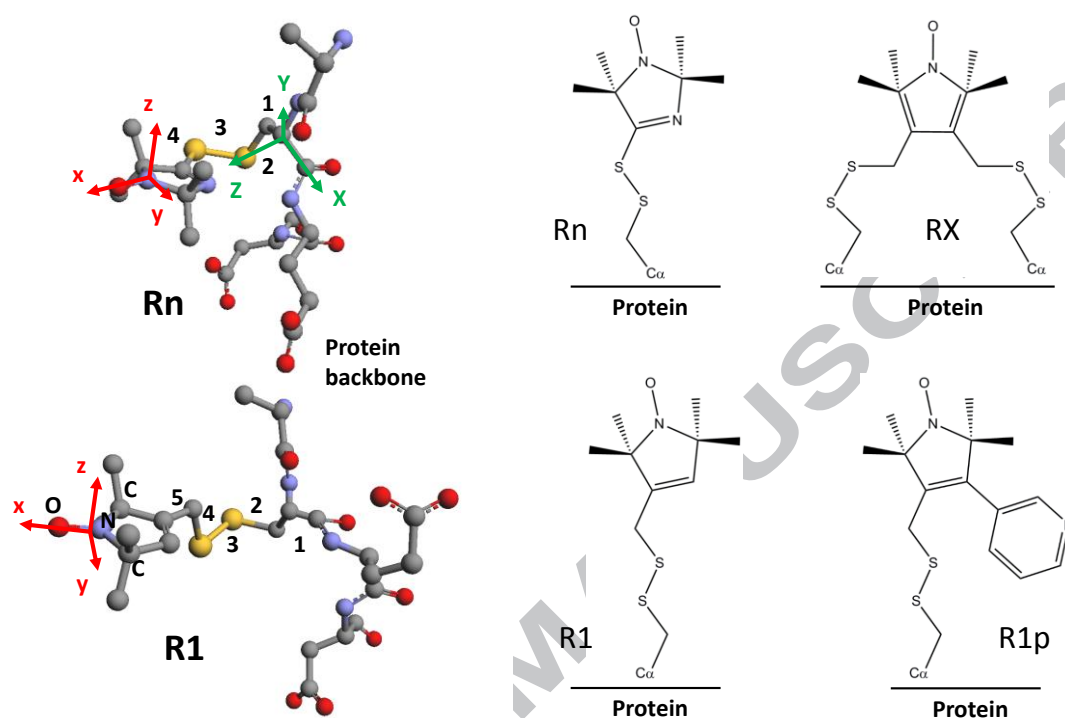


**Figure 1.** Rn and R1 spin labels attached to a protein backbone via a cysteine residue. Dihedral angles of the tethers are indicated by numbers. Structures of R1p and RX spin labels are also included for comparison. Magnetic axes of the nitroxyl and nitroxide head groups and protein fixed axes are indicated by red and green arrows, respectively, where  $x$  axis of the magnetic frame lies along the N-O direction.

distribution can significantly complicate both the analysis and interpretation of CW EPR spectra and long-range distance measurements in proteins using pulsed EPR techniques (11). For this reason SLs having fewer rotameric states and more restricted internal mobility should have greater utility. Examples previously employed include introduction of a bulky substituent in the nitroxide ring (12), generation of a second covalent bond between the nitroxide ring and the protein backbone (6, 13) and genetically encoded artificial amino acids for labelling specially synthesised probes (14). For instance, Fawzi et al. have reported a modified disulphide-linked label R1p, as an alternative to the flexible labels, with the

pyridine ring attached to the nitroxide group (15). Such a modification significantly reduces internal mobility assuming a single rotamer on solvent exposed helical surfaces reported in their paper. More recently, Hubbell and co-workers have reported the introduction of nitroxide spin probe (RX) linking to the protein via two cysteine residues (16) with highly constrained motion. However, such spin probes are not straightforward in sample preparation and may significantly perturb the local structure of the protein (13, 14).

The bi-radical bis-(2,2,5,5-Tetramethyl-3-imidazoline-1-oxyl-4-yl) disulfide ( $R_nSSR_n$ ) was developed in 1989 primarily for the quantitative determination of sulfhydryl (SH) groups using EPR(17-19). Since it reacts readily with the thiol side-chain of cysteine protein residues it has potential utility as a probe of motion although this has been little explored. Since the tether of  $R_n$  (Figure 1) to the protein has only four atoms compared with the five of MTSL it possesses a total of only 18 rotameric states compared to 108 states in the case of  $R_1$ . This suggests it will be easier to disentangle the tether motional constraints from those of the surrounding protein. Moreover, the partial double bond character of the C-S link between the tether and the nitroxyl ring system of  $R_n$  yields a higher barrier to rotation about this bond than in MTSL.

The purpose of this study is to provide useful insights into the local dynamics of both the widely used MTSL ( $R_1$ ) spin probe and the less well explored  $R_n$  nitroxyl probe. We have performed a combined EPR and fully atomistic MD simulation study of both SLs attached to sperm whale Myoglobin (Mb) at two surface sites S58C and S117C, respectively, shown in Fig. 2. Here we provide evidence, based on both experimental observations and molecular modelling, that  $R_n$  is, indeed, a useful spin probe more sensitive to the local protein environment than  $R_1$  in terms of EPR lineshape changes as a function of local protein structure. By performing a comparative study of the dynamics and EPR spectra of both labels attached at structurally different sites of Mb we conclude that for S58 site the internal

mobility of Rn is significantly restricted compared to R1 thus making Rn a more sensitive probe of the protein motion.

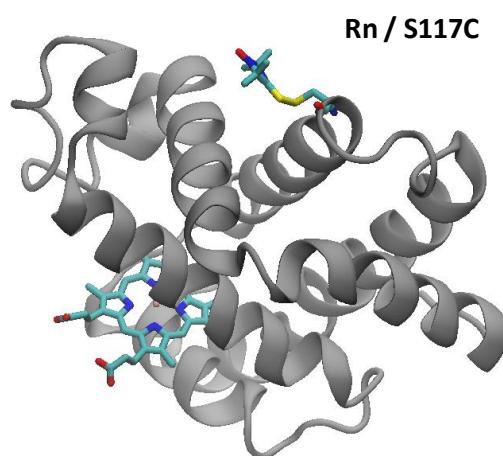
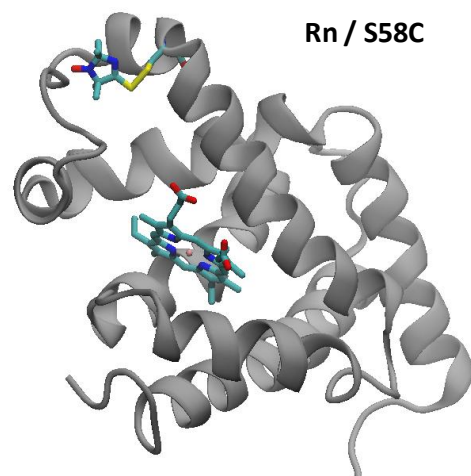


**Figure 2.** The complete structure of Mb, with the protein backbone displayed as a ribbon, showing the heme group and the positions of C58 and C117 with the Rn spin label attached.

## Materials and Methods

### Computational methods

#### *MD simulations*

The structure of myoglobin was taken from the PDB databank (code PDB 1MBO). Serine residues S58 and S117 were substituted by cysteine residues. Spin labels with tethers, Rn and R1, derived from RSSR and MTSL, respectively, were attached via disulfide bridges to the thiol sidechain of cysteine 58. Spin labelled myoglobin was solvated in a truncated octahedral box of the TIP3 water model (~3000 solvent molecules). The Amber force field ff99SB (20), specifically tailored for biological systems, was used to model the protein and extended by including a new parameterisation for both R1 and Rn as non-standard residues. The sets of force field parameters for the nitroxide and nitroxyl groups of R1 and Rn, respectively, were adapted from Barone and co-workers (21, 22) (Tables S1-S8 of Supporting material). For the tethers of both labels, the dihedral angles 3, 4 and 5 and 3 and 4 for R1 and Rn, respectively, were determined by fitting to QM potential energy scans. The remaining two torsions -S-S-CT-CT- (angle 2) and -S-CT-CT-N- (angle 1) were assigned to similar parameters in the force field. The ESP partial charges for the spin labels were calculated from their optimised structures at B3LYP/6-311G\*\*, using the CGhelp method in Gaussian 09 (23). For the heme moiety of Mb, Amber parm 94 and Giommona's parameters were used (<http://pharmacy.man.ac.uk/amber/>) (24). Hydrogen atoms were added to the structure with the protonation state of histidine residues corresponding to pH = 7. Cl<sup>-</sup> counter ions were added to neutralize the total charge of the protein. All MD simulations were performed in the canonical (NVT) ensemble at 300 K for equilibration followed by production runs in the NPT ensemble at 1 atm and  $T = 295$  K by using the Particle mesh Ewald molecular dynamics (PMEMD) module of the Amber11 package (25). Langevin dynamics with a collision frequency of  $2.0 \text{ ps}^{-1}$  were used to control the temperature. The equations of motion were integrated for >500 ns with a time step of 1fs. Periodic boundary conditions and the particle mesh Ewald (PME) method were applied to account for long range interactions in explicit

solvent. The production output using a multi-processor parallel cluster was typically ~5ns of a MD trajectory per day.

The EPR spectral line shapes of nitroxide spin labels are determined entirely by the variation with time of two angles that define the orientation of the applied magnetic field to the principle axis of the nitroxide group. Therefore, the orientational history of the z axis of the nitroxide ring (coincident with the direction of  $p_z$ -orbital of N) is calculated from the cross-product of the unit vectors of N-O and N-C bonds (see Figure 1) (26).

### ***Modelling of the global rotational diffusion (GRD) of Mb***

The lengths of the MD trajectories, even as long as 500 ns employed in this study, do not allow adequate sampling of all evenly distributed orientations of the tumbling protein in solution. This degrades the quality of the simulated rotational correlation functions and EPR lineshapes. In addition, it is known that the TIP3 water model in MD simulations overestimates the viscosity of water that affects the global tumbling of the protein molecules in solution and associated correlation times (27). The latter point is illustrated in Figure S1 of Supporting material that compares the correlation functions of the Z-axis of two protein fixed frames calculated from the two 500 ns MD trajectories (red and blue lines) with the one generated from a model dynamical trajectory (Brownian Dynamics (BD) trajectory) of isotropic tumbling with 9.7 ns correlation time for Mb (green line). A time scaling factor of ~1.5 applied to the MD trajectories was required to match the curves. It is common practice to remove global tumbling of the protein from the MD trajectories and re-introduce it by a BD approach (11, 27, 28). In order to achieve an accurate representation of the global tumbling of the protein molecule the BD trajectories for Mb were obtained by direct numerical solution of the Langevin equation (29, 30) corresponding to the rotational diffusion described by three rotational diffusion coefficients  $D_i$  for the reorientations of the

protein molecule around its internal axes. For an isotropic rotational diffusion the following relationship between the diffusion coefficient and correlation time was used:  $\tau = \frac{1}{6D}$ . An in-house built computer program (26) was employed to generate BD trajectory. The correlation time of the isotropic rotational diffusion of Mb (9.7 ns) was taken from the literature (31). A sufficiently long 2000 ns single BD trajectory representing GRD was generated in order to provide enough statistical points for averaging using 'sliding time window technique' (26).

***Building up long total dynamical trajectories for EPR spectral simulations.***

MD trajectories associated with pure spin label dynamics were extracted by coordinate transformation of the magnetic axes of nitroxide from the laboratory frame to the protein backbone frame which is fixed relative to the atoms in the chain (Figure 1). The Z-axis of the protein frame is perpendicular to the plane defined by the carbonyl  $C_\alpha$  atom and its neighbouring N and C atoms. The X-axis is chosen to be along  $C_\alpha$ -C bond and the Y-axis is the vector product of the previous two.

In order to match the length of the BD trajectory representing GPD all extracted MD trajectories were extended using time reversal approach (32). As has been demonstrated previously (32) the working length of the MD trajectory can be extended several times by taking the advantage of the fact that the classical equations of motion are reversible in time. Thus time is used as an extra "degree of freedom" to provide additional points (26, 32).

Hence, one can effectively at least quadruple the length of the working trajectory:  $T_{ext} = [T; -T; T; -T]$ . Note that such a procedure does not improve conformational or kinetic sampling of the label and serves only to extend dynamical trajectories continuously. Resulting extended MD trajectories with lengths >2000 ns have then been superimposed on

the long BD trajectory representing GPD by applying Cartesian transformations and then used directly to predict the EPR spectra using our general simulation methodology (26).

***Building up trajectories corresponding to spin label dynamics excluding rotameric flips.***

This was achieved by selecting sections of the trajectory where no dihedral flips occur amongst any of the dihedral angles and choosing only one rotameric mode of motion (similar behaviour was observed for different selected sections). For such trajectory segments firstly the rotations of magnetic axes in the laboratory frame have been transformed into the protein fixed frame and then extended to the total length of 2000 ns using a time-reversal approach as described above (26, 32). Finally, this trajectory in the protein frame was superimposed with the GPD trajectory.

***Simulation of EPR spectra***

Finally, the total 2000 ns MD-GPD trajectories are transferred into an EPR simulation program, developed and described previously by one of us (26, 32), that calculates the variation in time of the averaged transversal magnetisation and, eventually, the EPR line shapes. According to this approach an accurate simulation of the transfer magnetisation is achieved from a single dynamical trajectory (DT) until the point when the autocorrelation function of re-orientational motion of spin label has completely relaxed. Statistical averaging is achieved by the “sliding time window technique” allowing the use of single MD trajectories for predicting EPR line shapes. Homogeneous line broadening was taken into account with the relaxation parameter  $T_2 = 0.22 \mu\text{s}$ , as previously described (26, 32). The following principle values of  $\mathbf{g}$  and  $\mathbf{A}$  hyperfine coupling tensors were employed for both labels:  $g_{xx} = 2.0085$ ;  $g_{yy} = 2.0065$ ;  $g_{zz} = 2.0026$  and  $A_{xx} = 6.0\text{G}$ ;  $A_{yy} = 6.0\text{G}$ ;  $A_{zz} = 35\text{G}$ . Because of the relatively long total MD times generated in this work we have also attempted the simulation of EPR spectra by propagation of the spin density matrix along long sampling

times. The resulting spectra give similar results. A program written in-house was used for all simulations and analysis of EPR spectra by both approaches (26).

### *Calculation of correlation times*

The calculation of effective correlation times was carried out using the following expression:

$$\tau = \int_0^{\infty} C'(t) dt \quad (1)$$

where  $C'(t)$  is properly normalised auto-correlation function  $\langle D_{00}^2(\Theta(0))D_{00}^2(\Theta(t)) \rangle$  defined using an associated Wigner rotational matrix element  $D_{00}^2 = (3\cos^2 \Theta(t) - 1)/2$ .

$C'(t) = (C(t) - C(\infty)) / (C(0) - C(\infty))$ , in order to satisfy the following conditions:  $C'(0) = 1$  and  $C'(\infty) = 0$ .

### *Transition based assignment (TBA) of dihedral states in R1 and Rn spin labels.*

Dihedrals of spin labels are defined as follows: For MTSL (R1):  $\chi_1 = \text{S-CT-CT-N}$ ;  $\chi_2 = \text{S-S-CT-CT}$ ;  $\chi_3 = \text{CT-S-S-CT}$ ;  $\chi_4 = \text{CC-CT-S-S}$ ;  $\chi_5 = \text{CP-CC-CT-S}$ ; For Rn:  $\chi_1 = \text{S-CT-CT-N}$ ;  $\chi_2 = \text{S-S-CT-CT}$ ;  $\chi_3 = \text{CT-S-S-CT}$ ;  $\chi_4 = \text{CP-CC-S-S}$ .

For each moment of time dihedral states have been coarse-grained using TBA reported previously for amino acids in proteins (33) and spin labels (34). According to this approach, the states are assigned with the help of transition paths which connect well-defined regions in the rotational space, and the transition takes place only when the trajectory crosses from one band to another. Hence fast non-Markovian fluctuations do not contribute to a state change.

The stringent condition of  $\pm 20^\circ$  for all dihedrals was used to generate auxiliary binary functions used in the analysis of dihedral motions.

***Introduction of the binary functions for the evolution of coarse-grained dihedral states and calculating covariance matrices among different dihedrals.***

After TBA for each dihedral states a binary function of time,  $F(t)$ , has been introduced and built using the following rule. For each incremental time  $t$ :

1.  $F(t) = 1$ , if dihedral changes from one coarse-grained states to another
2.  $F(t) = 0$ , otherwise

Such a binary function can be effectively and straightforwardly used in the calculation and analysis of cross-correlations among different dihedral flips as well as the speeds of such changes. We define the covariance matrix  $\mathbf{M}$  (cross-correlation matrix at the lag time 0) as follows:

$$\|\mathbf{M}\|_{ij} = \sum_t F_i(t)F_j(t), \quad (2)$$

where indices  $i, j$  correspond to dihedrals ( $\mathbf{M}$  is 5x5 and 4x4 matrix for R1 and Rn, respectively) and the sum is taken over all incremental times  $t$ . A time step of 1 ns was used in the calculation of all covariance matrixes. For different pairs of dihedrals this matrix provides the numbers of simultaneous rotameric changes between them during the total sampling time. From the  $\mathbf{M}$  matrices the total number of rotameric changes  $N$  over the sampling time can be calculated using the following expression:

$$N = 2Tr(\mathbf{M}) - \sum_{i,j} M_{ij} \quad (3)$$

## **Experimental methods**

### ***Preparation of cysteine variant of Myoglobin***

Both the S58C and S117C variants of recombinant sperm whale myoglobin were expressed from the plasmid pMb413 (35). The plasmid DNA sequence was validated by MWG Biotech ComfortRead assays. The protein was prepared and purified using the method described by Springer and Sligar (35). The final protein solution was exchanged via Amicon into 20mM HEPES pH7 buffer that had been de-ionised by passage over CHELEX 100 resin. At this stage the product contained a mixture of oxidation states so the protein concentration was estimated from the absorbance at 280 nm where the reported extinction coefficient is approximately  $35,000 \text{ M}^{-1}\text{cm}^{-1}$  for both oxymyoglobin ( $\text{Mb-Fe}^{2+}(\text{O}_2)$ ) and metmyoglobin ( $\text{Mb-Fe}^{3+}(\text{H}_2\text{O})$ ) (36).

### ***Spin Labelling***

(S-(2,2,5,5-tetramethyl-2,5-dihydro-1H-pyrrol-3-yl)methyl methanesulfonothioate) (MTSL) was purchased from Toronto Research Chemicals, Canada. HEPES, CHELEX 100 and Dithiothreitol (DTT) were from Sigma-Aldrich, UK. De-salting columns filled with Sephadex G-25 (PD10 columns) were obtained from Amersham Biosciences, UK. Samples of Myoglobin labelled with MTSL were prepared according the procedure described previously (32).

A quantity of bi-radical RnSSRn was donated by Prof. Valery Khramtsov from West Virginia University. The nitroxyl spin label RnSSnR (Rn) is the bi-radical bis-(2,2,5,5-tetramethyl-3-imidazoline-1-oxyl-4-yl) disulfide. This label exchanges readily with other thiols including the side chains of exposed cysteine residues. The SL was added as a solution in acetonitrile to 2.5ml protein in 20mM HEPES pH7 buffer to give a 10:1 label to protein ratio. The mixture was foil wrapped and incubated at room temperature for 30 minutes with gentle mixing. Excess spin label was removed by treatment with two successive PD10 columns followed by concentration using centrifuge-spun micro-concentrators.

Protein concentration was  $\sim 50 \mu\text{M}$  in all samples and was determined by absorption at 280 nm. Spin label concentration was checked by comparing the integrated EPR absorbance spectrum of spin labelled proteins with that of an MTSL standard. The degree of labelling was greater than 95% in the case of R1 and was approximately 35% in the case of Rn.

During the sample preparation and EPR measurements the following has been observed. Portions of Mb were incubated with R1 and Rn labels using identical conditions. PD10 desalting columns were then used to separate spin-labelled protein from any residual free label. After two successive column treatments there were almost no features associated with rapidly-tumbling, free spin label in the EPR spectrum of R1 labelled Mb. However, for Rn labelled Mb, features characteristic of rapidly-tumbling, free label were observed in the EPR spectrum after each column treatment, indicating that Rn is reversibly bound to the protein and is in equilibrium with free label. We attribute the observed lower binding strength of Rn to the cysteine compared to R1 to both the shorter side chain of Rn and, as discussed below, the higher torsional barrier of the dihedral that connects its head group to the linker. Because of both factors Rn is most likely to be constrained by interactions with neighbouring amino acid residues inhibiting its attachment to protein.

Example of EPR spectrum with free label contribution is shown in Figure 3 for S117C site. Thus, after each column treatment, Rn is released from the protein so that the proportion of free label is maintained as the concentration is reduced. The Rn probe linkage to cysteine is stable under neutral pH conditions with only  $\sim 2\%$  of the estimated free label relative to the label bound form detected in solution (See Figure 3). No change in the EPR spectrum of the labelled protein was detected after  $\sim 7$  hours at room temperature. The fast motion component arising from free Rn, shown in blue in Fig. 3, has been simulated from generated BD trajectory with  $\tau = 0.02$  ns correlation time and homogeneous line broadening  $T_2 = 0.83 \mu\text{s}$ . Numerical simulations of both slow and fast motional contributions allow estimation of the

relative amounts of the two components in the spectra for Rn spin label. A similar procedure was performed for the total spectrum of Rn at S58C site.

The experimental spectra corresponding to Mb labelled with Rn shown in Figure 4 have been obtained by extracting fast motional contribution from the total spectrum.

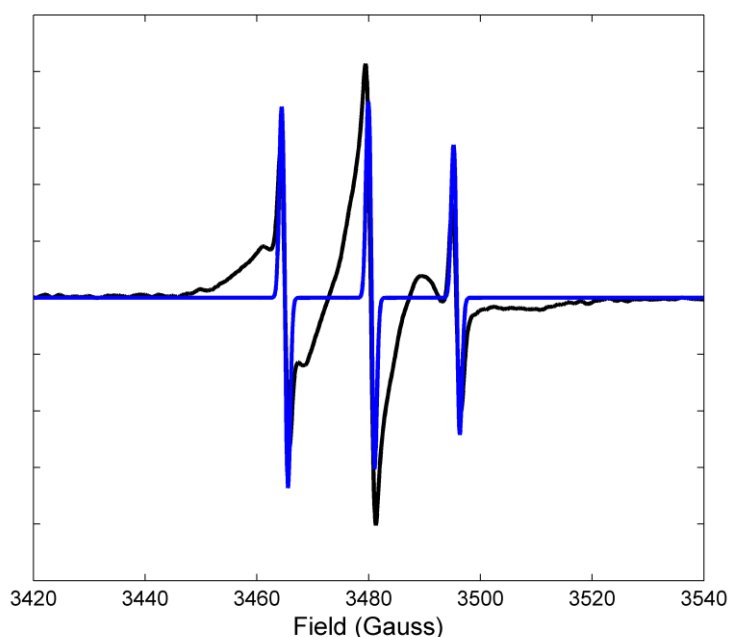


**Figure 3.** Total EPR spectrum of Rn attached at S117C site after keeping the sample for ~7 hours at room temperature (black line). The fast motion component arising from free Rn, shown in blue, was simulated using BD trajectory of isotropic motion with  $\tau = 0.02$  ns correlation time.

### *EPR measurements*

Room temperature EPR spectra were measured using an X-band Bruker EMX spectrometer fitted with the ER4102ST resonator used in combination with the 19-bore AquaX cell for measurements on aqueous samples. The following conditions were used: microwave power of 2 mW; modulation frequency of 100 kHz; modulation amplitude of 1.0 G.

## Results and Discussion

### *Comparison between predicted from MD and experimental EPR spectra of Rn and R1 spin labels*

Figures 4 a) and b), top lines, show the experimental CW X-band EPR spectra of R1 attached at sites S58C and S117C, respectively. The spectra are very similar to each other with lineshapes characteristic of highly mobile rotameric dynamics of R1 positioned at a protein-solvent interface. In contrast, the experimental spectra of Rn (top lines in Figs 4 c) and d)) attached at the same sites are both broader compared to R1 spectra corresponding to a slower motional regime although the label Rn at 58C site is clearly the less mobile. Also noticeable, at site S117 the spectrum of Rn is distinctly broader compared to the one of R1 indicating lower degree of the label sidechain mobility.

MD simulations are today faster and more accurate thus gaining predictive powers and providing an important tool complementary to experiments (37). Recently, novel approaches have been introduced that allow the prediction of motional EPR spectra from MD trajectories (4, 26-28, 38, 39). This can greatly simplify the interpretation and analysis of experimental results, and hence provide unambiguous conclusions about molecular order and motions. These methods have been successfully applied to soft matter systems doped with nitroxide spin probes (40, 41) and MTSL spin labelled proteins (4, 26, 28, 32, 38). In order to probe motions of both R1 and Rn in two different protein environments and to predict and analyse the relevant EPR spectra we have performed fully atomistic MD simulations of all four cases of spin labelled Mb.

First, we have developed an accurate set of force field (*ff*) parameters for both probes. Details of the *ff*s and MD protocols are provided in Supporting material. A set of long MD simulations runs (>500 ns) using the AMBER 11 simulation suite (25) has been performed.

The generated MD trajectories were converted into the protein reference frame and finally superimposed with the BD trajectory for the GRD of the Mb generated as described above. The latter represents the isotropic rotational diffusion of Mb with the known correlation time of 9.7 ns obtained by  $^1\text{H}$  NMR spectroscopy (31). Finally, the dynamical trajectories were used to predict EPR spectra according to the general MD-EPR simulation procedure (26, 32).

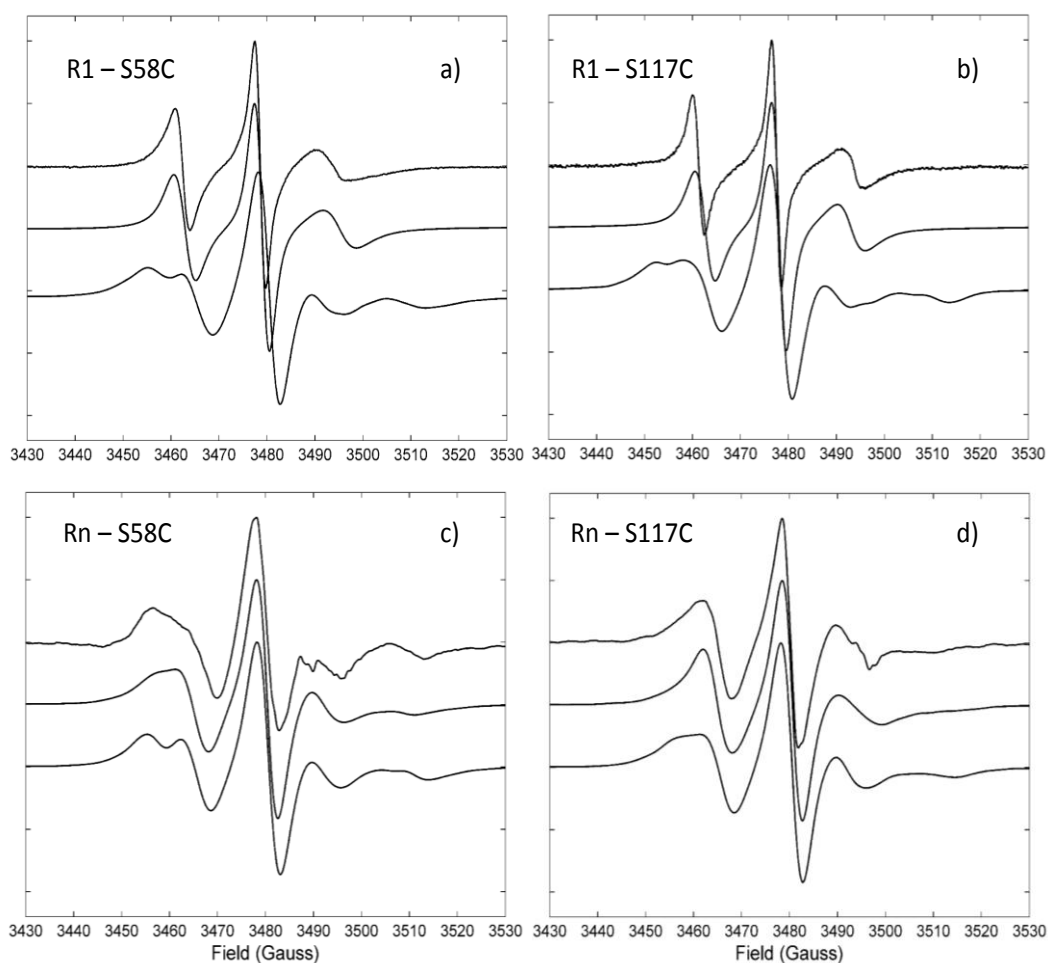


**Figure 4.** Comparison between experimental and simulated EPR spectra for R1 and Rn at two sites of attachment in Mb. In each panel top, middle and bottom lines correspond to experimental spectrum, spectrum predicted from MD and the one predicted with rotameric dynamics excluded, respectively. In the experimental spectra of Rn fast motional contribution from the free label has been removed using a procedure described in Experimental section.

The predicted spectra for all four combinations, namely R1 at S58C, R1 at S117C, Rn at S58C and Rn at S117C sites ( shown as middle lines in panels a), b), c), d), respectively, of Fig 4) are in good agreement with experiment reproducing all the characteristic features of the lineshapes in the relevant fast and slow motional regimes. The predicted spectra confirm the fast dynamics of R1 label at both sites of attachment with the very similar line shapes. Simulations also reveal the much slower dynamics of the Rn spin label at site S58C confirmed in the experimental spectra by the presence of additional features at low and high magnetic fields, namely the peak and trough observed at  $\sim 3455$  G and  $\sim 3512$  G, respectively (Fig 4c). Although there are some discrepancies observed between the predicted and experimental EPR spectra the predicted spectrum captures very well all the main features of the experimental line shape. This includes the positions of both the inner and outer peaks at  $\sim 3470$  G and  $\sim 3490$  G and at  $\sim 3455$  G and  $\sim 3512$  G, respectively, of the axially symmetric motionally averaged hyperfine coupling. The difference between outer peaks ( $2A_{zz}$ ) is a particularly sensitive parameter to the dynamics of the molecule in the slow motional regime (1, 5, 7).

#### ***Impact of different motional contributions on the EPR lineshapes of Rn and R1 labels***

The advantage of using MD simulations at the atomistic level to predict EPR spectra is the ability to extract, and inspect, separately, different motional contributions to the overall dynamics of the label. Thus there are three contributions to the overall re-orientational dynamics of a SL that define the unique shape of the EPR spectra (26, 27, 32). The first comes from the librational motions associated with oscillations around the dihedral angles of equilibrium states in the range of  $\pm 30^\circ$  (11) with the observed excursions up to  $\pm 45^\circ$  (26). These motions allow the label to explore the conformational mobility around individual rotameric states (up to  $\sim 100$  ps). The second type of motion is predetermined by the

rotameric stochastic dynamics when flips occur among different sets of dihedral angles (rotameric states). The third contribution comes from the protein dynamics, both local and overall tumbling motions. Librational motions fall within the so-called fast EPR motional regime at X-band ( $< 0.5$  ns) while the rotameric dynamics is normally within the intermediate ( $0.5$  ns –  $3$  ns) and slow ( $3$  ns –  $100$  ns) EPR motional regimes. Protein motions are either within the slow motional regime or completely immobilised on the EPR timescale.

Figure 5 represents calculated from MD auto-correlation functions of the re-orientational motions of the z-magnetic axes of both Rn and R1 spin labels. They confirm not only the relatively fast dynamics of R1 (blue lines in both panels of Fig 5) but also show the slower but different motions of Rn at the S58C and S117C sites (red lines in panels a) and b), respectively). All the auto-correlation curves presented in Figure 5 clearly show bi-exponential behaviour which is an indication of the different time scales of the motional contributions to the overall dynamics of the label, one from fast librational motions around rotameric

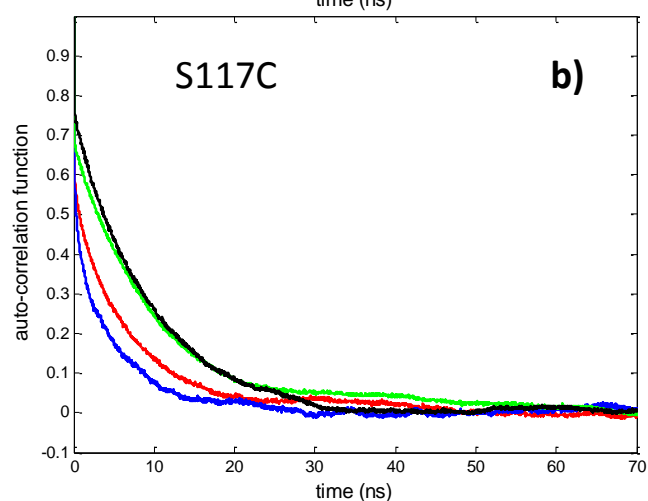
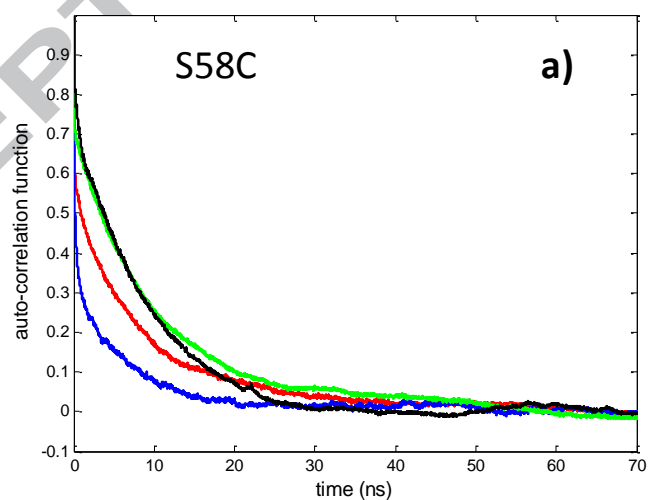


**Figure 5.** Rotational auto-correlation functions for the magnetic z-axes of Rn and R1 spin labels, shown as red and blue curves, respectively, attached at sites S58C (a) and S117C (b). Green and black lines represent auto-correlation functions of the z-axes of Rn and R1, respectively, generated from MD trajectories excluding rotameric dynamics.

modes and the other one from the combined dynamics of the tether and the protein. By integrating these curves (according to the equation (1)) the effective correlation times are calculated to be as follows:  $\tau_{R1-S58C} = 2.78 \text{ ns}$ ,  $\tau_{R1-S117C} = 2.80 \text{ ns}$ ,  $\tau_{Rn-S58C} = 5.70 \text{ ns}$ ,  $\tau_{Rn-S117C} = 4.40 \text{ ns}$ .

In order to illustrate the impact of the rotameric dynamics of the tethers of R1 and Rn on the EPR line shape their effects were excluded from the relevant MD trajectories. This was achieved by selecting sections of the trajectories where no dihedral flips occur amongst any of the dihedral angles and selecting only one rotameric mode of motion (similar behaviour was observed for different selected modes of each label). The results are presented in Fig 4 (bottom lines in each panel) and Fig 5 (black and green lines). There is a strong similarity between the resulting EPR lineshapes in all four cases (bottom lines in the panels of Fig 4) which are characteristic of a slow motional regime (7). Note that the EPR lineshapes with and without rotameric dynamics are close to each other in the case of Rn at S58C. The results are supported by the relevant auto-correlation functions, shown in Fig. 5 as green and black lines for Rn and R1, respectively, with all four resulting curves being almost identical to each other. Their effective total correlation times have the following values:  $\tau_{R1-S58C} = 6.50 \text{ ns}$ ,  $\tau_{R1-S117C} = 6.95 \text{ ns}$ ,  $\tau_{Rn-S58C} = 7.50 \text{ ns}$ ,  $\tau_{Rn-S117C} = 7.14 \text{ ns}$ . For R1 significant but

similar changes from the original curves are seen for both sites of attachment (black vs. blue line in both panels of Fig 5). Importantly, in the case of Rn, upon exclusion of rotameric dynamics, a more pronounced change is observed for site 117C (green vs. red line in panel b) of Fig 5) compared to 58C (green vs. red line in panel a) of Fig 5).

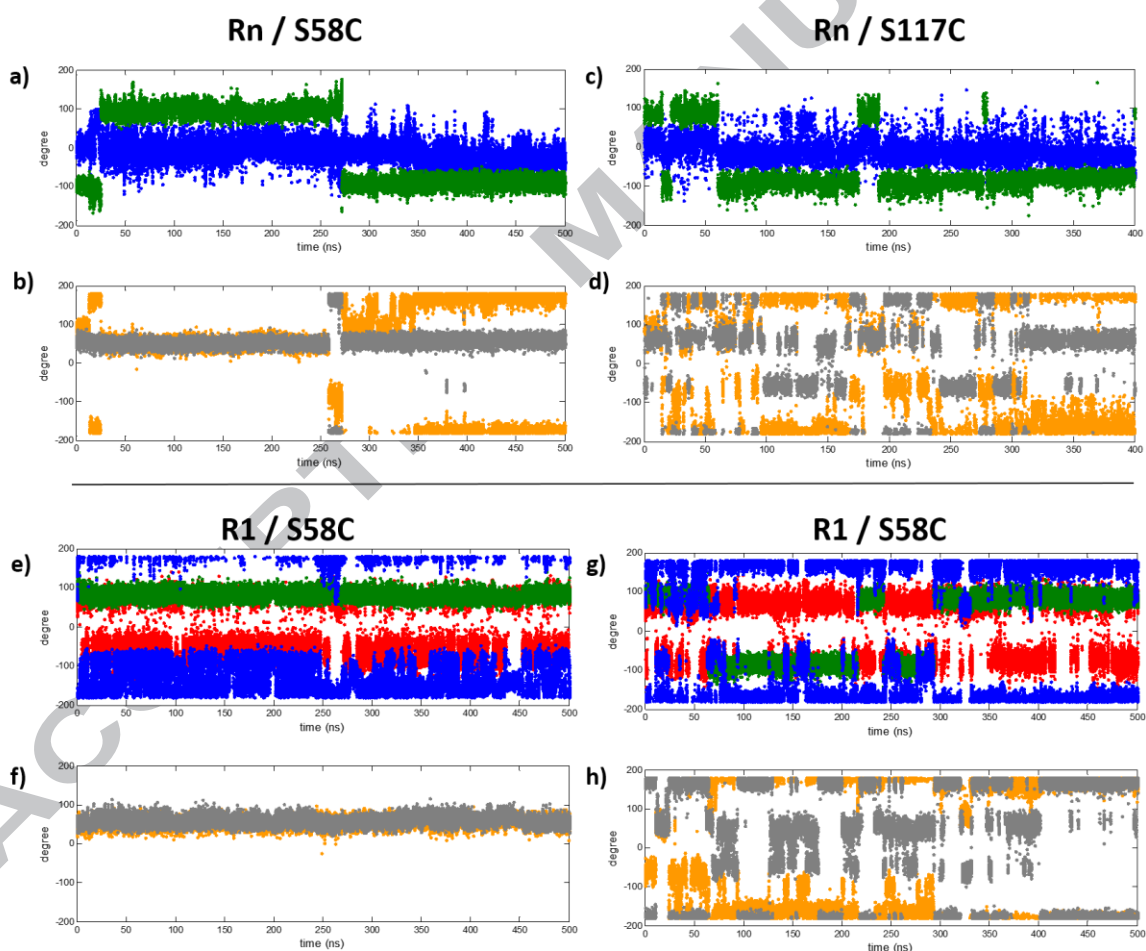


**Figure 6.** Time evolution of the dihedral angles of Rn and R1 spin labels; Panels on the left and right correspond to S58C and S117C sites of attachment, respectively; In both labels Rn and R1 dihedral angles  $\chi_1$ ,  $\chi_2$ ,  $\chi_3$ ,  $\chi_4$  are shown in grey, orange, green and blue, respectively. In R1 the dihedral angle  $\chi_5$  is shown in red.

*Analysis of rotameric dynamics of the sidechains in Rn and R1 at two sites of attachment.*

The above results show that the EPR line shape of Rn is a more sensitive function of the protein environment than that of R1 label. Further support comes from the comparison between, and analysis of, the calculated time evolution of the dihedral angles in Rn and R1 that are shown in Figure 6. In addition, we have carried out coarse-graining of the dihedral states using Transition based assignment (TBA) approach for spin labels (34) and the introduction of special binary functions to characterise dihedral flips (equations (2) & (3)). These functions are used to calculate covariances, the measure of how much two stochastic variables change together, between different pairs of dihedral angles in each case. The results are shown in Tables 1 and 2 for Rn and R1 labels, respectively. Both residues C58 and C117 lie on the surface of Mb exposing attached labels to solvent (42). However, the interactions of the labels with the local surrounding protein differ. These differences have a pronounced effect on the motional X-band EPR spectra of Rn at both sites but not on the R1 label at either site. Site S58C is located on the loop that connects two alpha-helices in Mb. As a result both labels experience steric constraints by the surrounding amino acid side chains. The hindered local environment of C58 limits the Rn label motions to 4 distinct

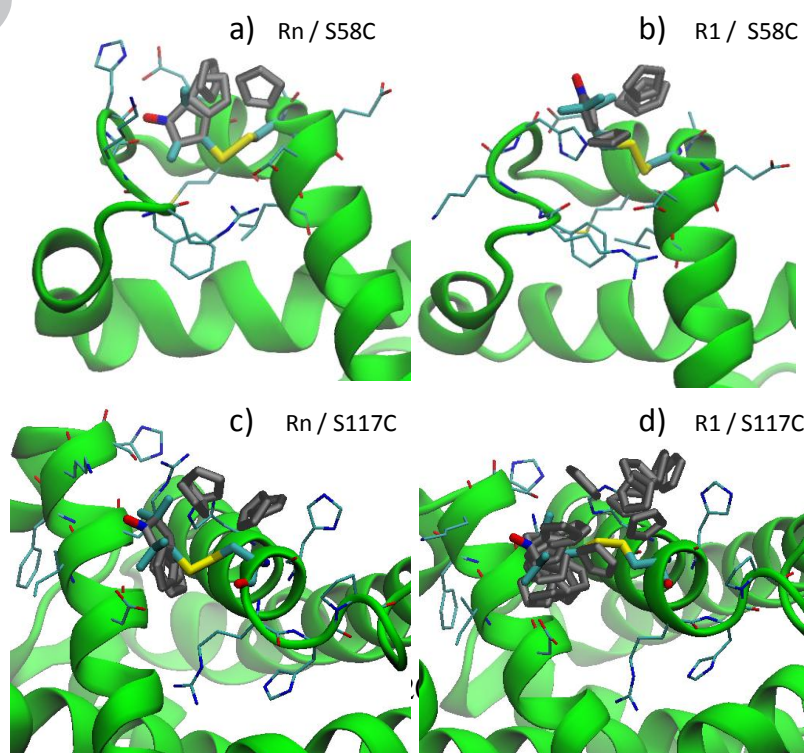


**Figure 7.** Rotameric states of Rn and R1 at sites S58 and S117 detected over the periods of 500 ns. In each panel the states are represented by the super-positions of either nitroxide or nitroxyl rings (gray colour). All sidechains have been deleted for clarity except, in the case of S58C, R45, F46, K47, H48, E54, M55, A57, E59, D60, L61, and in the case of S117C, H113, H116, R118, H119, P120, D27, I30, R31, F33, K34, S35, H36.

conformations (Fig 7a) with only 19 flips among them over 500ns time scale (slow rotameric exchange) (Fig 6 a) and b) and Table 1). At the same site MTSL (R1) also has a small number of conformations (6 as shown in Fig 7 b), defined predominantly by dihedrals  $\chi_4$  and  $\chi_5$  but by contrast the exchange between them is very rapid, on a sub-nanosecond time scale (525 flips mainly among highly correlated dihedrals  $\chi_4$  and  $\chi_5$  (Fig 6 b) & d) and Table 2). Thus the anisotropy of both tensors  $\mathbf{g}$  and  $\mathbf{A}$  in R1 is averaged out resulting in the significant narrowing of EPR lineshape. The case with site 58C is quite instructive for understanding the impact of the labels sidechain motions on the EPR lineshapes. As one can see from Fig. 6 e) and f) for R1 the dihedrals  $\chi_1$  to  $\chi_3$  are essentially locked compared to their counterparts in Rn and the motions of the label are entirely determined by the flips of dihedrals  $\chi_4$  and  $\chi_5$  resulting in the narrowed EPR lineshape similar to the one observed for S117C. This illustrates the impact of the dynamics of the dihedrals  $\chi_4$  and  $\chi_5$  in MTSL on the EPR lineshapes that reduces the sensitivity of R1 to protein motions and local structure. The situation is clearly different for Rn that has very restricted mobility for all its dihedrals at site C58 due to steric constraints imposed by the surrounding amino acids side chains that hinder concerted transitions of dihedrals  $\chi_1$ –  $\chi_3$ . In contrast, in R1 dihedrals  $\chi_4$  and  $\chi_5$  change independently from the rest and completely determine the averaging of the EPR lineshape at

site C58. In comparison with site C58, Rn bound to C117 is much less hindered by the local protein surroundings and, therefore, visits more conformations (9 as shown in Fig 7c) due to flexibility of dihedrals  $\chi_1$  and  $\chi_2$ , resulting also in a higher than in the case of C58 rate of flips (123 flips, see Fig 6 d) and associated covariance matrix in Table 1). R1 bound to C117 (Fig 7d)) also undergoes rapid inter-conversion among many states (21 in total with 429 flips among them) owing to the lack of hindrance from local protein structure that allows rapid sub-nanosecond dynamics now involving highly correlated motions of dihedrals  $\chi_1$ ,  $\chi_2$ ,  $\chi_4$  and  $\chi_5$  (see Fig 6 g) and h) and associated covariance matrix in Table 2). Yet the spectrum for MTSL at site 117C is almost identical to the one at 58C.

**Table 1. Covariance matrix among dihedral angles 1, 2 and 3 of Rn at sites S58C and S117C.**

	$\chi_1$	$\chi_2$	$\chi_3$
$\chi_1$	4 (91) <sup>a)</sup>	2 (39)	1 (4)
$\chi_2$		18 (70)	2 (3)
$\chi_3$			2 (8)

<sup>a)</sup> The matrix elements corresponding to S117C site are given in brackets;  $\chi_4$  is characterised by a single stable state and therefore is not given in the table. The unstable, close lying pseudo-states of  $\chi_4$  are excluded from the covariance matrix.

**Table 2. Covariance matrix among dihedral angles 1, 2, 3, 4 and 5 of R1 at sites S58C and S117C.**

	$\chi_1$	$\chi_2$	$\chi_3$	$\chi_4$	$\chi_5$
$\chi_1$	0 (241) <sup>a)</sup>	0 (10)	0 (5)	0 (14)	0 (40)
$\chi_2$		0 (44)	0 (1)	0 (30)	0 (16)
$\chi_3$			0 (5)	0 (1)	0 (1)
$\chi_4$				412 (99)	79 (20)
$\chi_5$					189 (178)

a) The matrix elements corresponding to S117C site are given in brackets.

For both labels, Rn and R1, angles  $\chi_1$ ,  $\chi_2$  and  $\chi_3$  have similar torsional potentials, unsurprisingly. Marked differences are, however, seen between the torsional potentials about angles  $\chi_4$ ,  $\chi_5$  of R1 and angle  $\chi_4$  of Rn. Our DFT calculations show that the dihedral angles  $\chi_4$  and  $\chi_5$  of R1 both have relatively low energy barriers to change of conformation of  $\sim 1$  and  $\sim 3$  kcal/mol, respectively (See Figure S2). These dihedral barriers determine the re-orientational mobility of the nitroxide ring of R1 and, hence, give rise to the characteristic EPR lineshape, particularly when bound at sites fully or partially exposed to solvent (26, 27, 32, 38). By contrast, torsion angle  $\chi_4$  in Rn has only single stable state at  $0^\circ$  with an energy barrier of  $\sim 8$  kcal/mol, the same value as the torsion about the S-S bond, dihedral  $\chi_3$  (27). The barrier about dihedral angle  $\chi_4$  arises from the partial double bond character of C-S due to the additional N atom in the nitroxyl ring (43). Formally a single barrier is associated with a single dihedral state. From Figure 6 a) and c) (blue lines) one can see that the distribution of angle  $\chi_4$  around its equilibrium value is in fact rather broad and must be influenced at each time by the values of other dihedrals resulting in the appearance of unstable closely lying pseudo-states. The rates of change of these unstable states are thus totally coherent with the flip rates of the dihedrals  $\chi_1$ – $\chi_3$  and do not increase the total rate of rotameric changes. Consequently, the overall rotameric dynamics of Rn are slower compared with those of R1. In this study relatively long conventional MD simulations runs of  $>500$  ns have been carried out in order to generate sufficient statistics for the dynamical and conformational sampling of the dihedrals. As has been highlighted and discussed in several recent reports (11, 27, 39, 44) some rotameric states can be under represented in conventional MD trajectories and more advanced MD simulations, e.g. those employing multiple trajectories with different starting conformations (27) or parallel tempering simulations such as Replica Exchange MD (REMD)

(34), would be required for adequate sampling to building up dynamical trajectories followed by the application of the kinetic modelling with either the Markov jump model (27) or the kinetic Monte Carlo algorithm (34). Importantly however, the rates of the concerted transitions which occur rarely and are not observed even in long conventional MD runs are also too slow on the EPR timescale. Yet the internal librational dynamics within such extra modes of motion may be different to the rest of rotameric states that are detected in the MD trajectory. As a result the contribution of such under represented modes into the total EPR spectrum might be different from the ones calculated from MD. This point can be illustrated, for example, by comparing the lineshapes simulated from four different single rotameric modes shown in Figure 4 as bottom lines. The lineshapes of these modes are very close to each other but not identical. We believe that such effects could be responsible for the minor differences observed between the experimental spectra and those predicted from single conventional MD trajectories reported in this study.

#### *Sensitivity of Rn and R1 spin labels to protein dynamics*

Both our experimental and modelling studies clearly demonstrate that Rn is a more sensitive probe to both protein dynamics and local structure as compared to R1 as traditionally employed. This is particularly evident for site S58C that has stronger effect on the internal dynamics of Rn compared to R1. The latter label is insensitive to the structural difference between the two sites of attachment. In order to demonstrate that the EPR lineshape of Rn at site 58C follows more closely the dynamics of protein we compare in Figure 8 a) the simulated lineshapes of both labels with the one generated from the trajectory of a pure Brownian rotational tumbling of Mb. Evidently, the EPR lineshape of Rn, shown in red, follows more closely the one corresponding to pure protein tumbling, shown in blue. In

contrast the lineshape of R1, shown in green, is strongly averaged out by the rotameric dynamics of the label.

The total protein dynamical contribution is a superposition of local backbone dynamics and the global protein tumbling. Thus for larger proteins with the tumbling correlation times being too slow on the EPR timescale ( $\tau > 100$  ns)  $R_n$ , in principle, would serve a better measure of the backbone dynamics. We have explored the differences among re-orientational dynamics of the two employed backbone fixed coordinate frames at two sites of attachment in Myoglobin and the frame attached to the heme plane with the z axis defined as its normal. The rotational autocorrelation functions calculated for the three frames are compared in Figure S1, after applying the time scaling factor. All three curves are very close to each other and match almost exactly the autocorrelation function generated from BD trajectory with a correlation time 9.7 ns indicating negligible difference in rotational motions among all three frames. Additionally, the autocorrelation functions of the x, y and z-axis of the S58C backbone frame were re-calculated in the heme frame and are shown in Figure S3. Apart from some small decay due to librational motions observed at short initial time the curves indicate high orientational order of all three axes in the heme frame concluding only minor differences between the motions of the backbone and the heme in Mb. The same situation is observed when the motions of the backbone frames are calculated relative to each other. This indicates very little difference in motion between the two backbones in Mb. Indeed, the EPR spectrum (not shown) calculated from the trajectory where the dynamics of  $R_n$  label at the site S58C is transferred to the heme frame and then superimposed with the GRD BD trajectory is indistinguishable from the original one. In order to illustrate the sensitivities of the EPR spectra from two labels to the protein dynamics we have compared in Figure 8 b) spectral lineshapes for both labels at site S58C calculated with 9.7 ns and 5 ns protein diffusional correlation times. While upon decreasing the protein correlation time almost

negligible change is observed for the spectrum of R1 there are noticeable changes in the lineshape of Rn indicating higher sensitivity of the latter to protein motions.

Finally, we have analysed the flexibility of Rn in terms of its interaction with the protein and how it perturbs the local protein structure compared to R1 label at the two selected sites of attachment in Mb. As have been pointed out previously (16) labels that are rigid, because of either the introduction of a bulky substituent in the nitroxide ring or the presence of the second covalent bond, are most likely to significantly perturb the local structure and also have relatively low sensitivity to small differences in nanosecond backbone dynamics of proteins compared to R1. We have performed a comparative analysis of the flexibility between R1 and Rn labels by comparing the equilibrated from MD structures of Myoglobin labelled with both

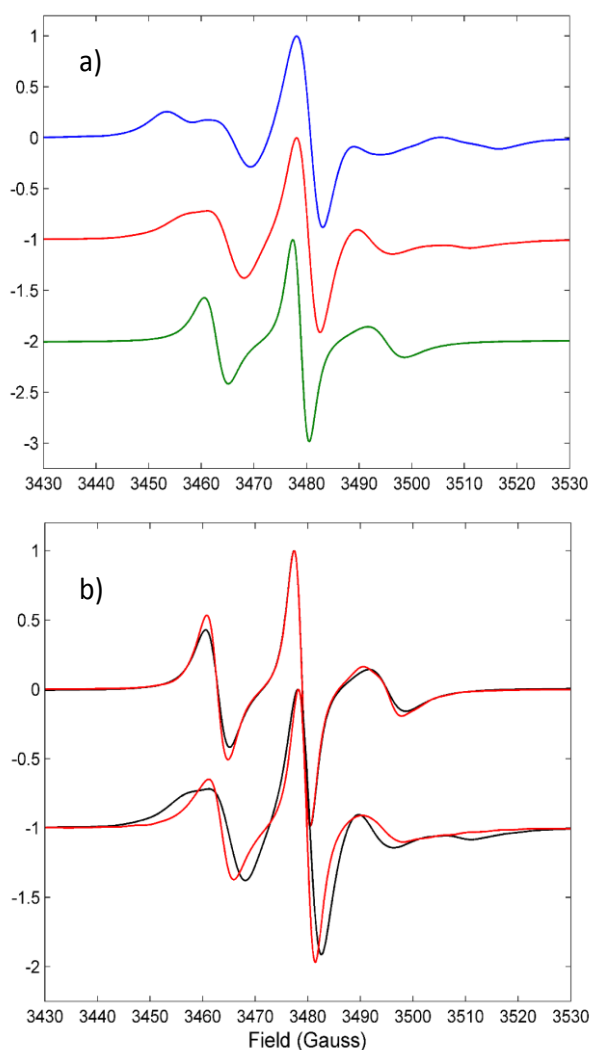


**Figure 8.** Panel a): Comparison between the EPR lineshapes simulated for R1 and Rn labels at site 58C, shown as green and red lines, respectively, and the one generated from the DT of a pure Brownian rotational diffusion of Mb excluding all label motions, shown as blue line. Panel b): Comparison between the EPR lineshapes simulated for labels R1 and Rn at site 58C using different protein tumbling motions. Top and bottom curves correspond to R1 and Rn labels, respectively. Within each pair red and black curves correspond to 9.7 ns and 5 ns protein diffusional correlation times, respectively.

R1 and Rn at two sites with its native structure. The results are presented in Figure 9. The calculated RMSDs of  $C_{\alpha}$  carbons between the native and labelled structures in each case were as follows: 1.4 Å (1.2 Å) and 1.3 Å (1.1 Å) for Rn and R1, respectively, at the site 58C and 1.0 Å (0.8 Å) and 1.1 Å (0.9 Å) for Rn and R1, respectively, at the site 117C. The RMSD values in brackets were calculated for selected parts of amino-acid sequences that contained the attached labels (residues 30-65 and 110-130 for sites 58C and 117C, respectively).

For comparison, the RMSD value calculated for  $C_{\alpha}$  atoms from the MD trajectory of the native Myoglobin structure is 1.1 Å. Both the aligned structures presented in Figure 9 and the calculated RMSDs of  $C_{\alpha}$  carbons confirmed similar effects from two probes on the protein structure.

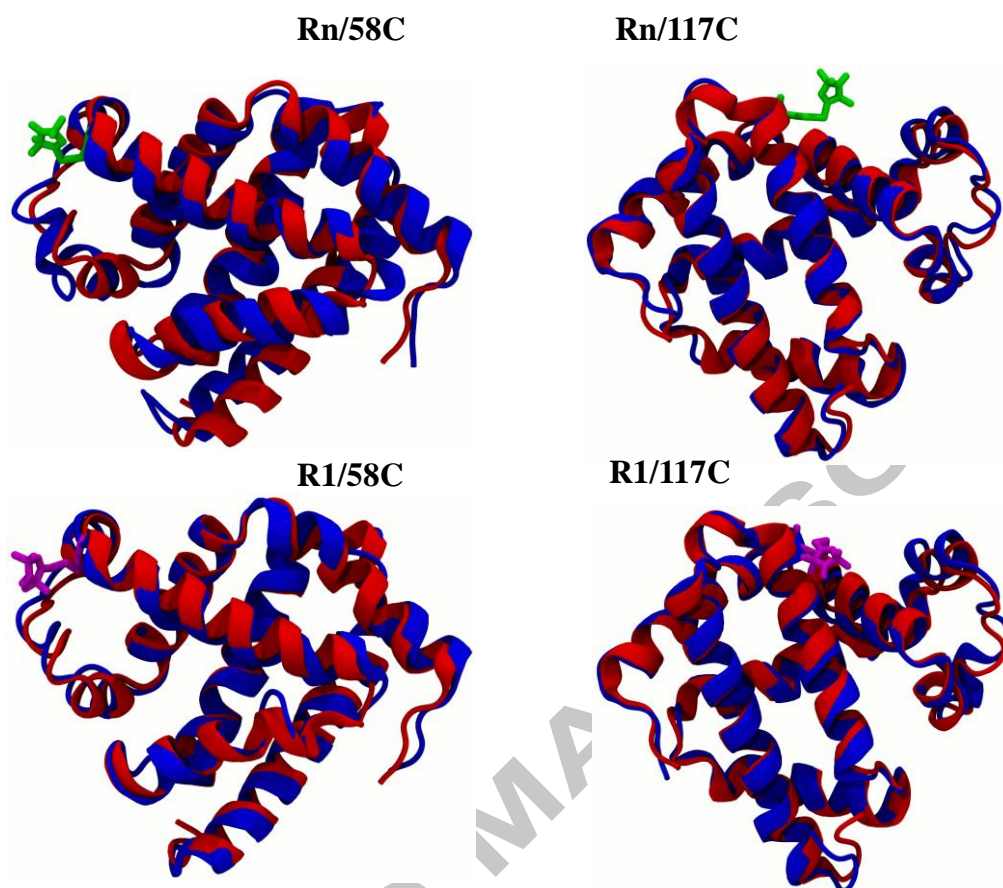


**Figure 9.** Alignments of equilibrated spin labelled (blue) and native (red) Myoglobin structures. Rn and R1 labels at two different sites of attachment are shown in green and purple, respectively.

### Conclusion

This study provides an insight into the dynamics of two protein spin labels with flexible tethers, namely R1, a widely used label in EPR studies, and Rn. Using state-of-the-art all atom MD simulations combined with CW X-band EPR we have provided evidence that the Rn is a sensitive probe to protein motion and the local protein environment. In particular, at the partially solvent exposed position S58C in Mb, where the EPR lineshape of R1 is significantly averaged out due to fast internal mobility, the rotameric dynamics of Rn is almost rigid having only a small effect on the EPR lineshape thus making Rn more sensitive to the protein dynamics. Analysis confirms that the strong averaging effects in R1 come

predominantly from the fast rotameric motions of dihedrals  $\chi_4$ ,  $\chi_5$  that can be fully uncoupled from the rest of dihedrals (site 58C). In contrast, in Rn the rotameric dynamics is predetermined by the angles  $\chi_1 - \chi_3$  which have relatively small rates. Comparative analysis suggests that Rn has flexibility similar to the one of R1 when the perturbation of local protein structure is concerned. The main features of Rn are thus as follows: i) Rn has rotameric mobility which is generally slower and thus more sensitive to protein dynamics and local environment compared to R1; ii) The flexibility of Rn is comparable to the one of R1 placing it in favourable position relative to highly rigid spin labels. Our results demonstrate that in cases where the dynamics of R1 is approaching fast motional regime with motional contributions averaged out Rn may offer a better choice to discern protein dynamics. This suggest the use of Rn in CW EPR experiments as a complementary probe to the widely applied R1 in order to provide a reporter on the protein that is more sensitive to a different range of dynamic behaviours.

**Author contributions:** VSO and AJT designed the research; VSO, FC and GW performed the research; VSO analysed data; VSO and AJT wrote the manuscript.

### **Acknowledgements**

We are grateful to Prof. Valery Khramtsov from West Virginia University for donating a sample of bi-radical RnSSRn. VSO gratefully acknowledges support from EPSRC (grants EP/H020411/1 and EP/L001322/1). The authors wish to thank the Research Computing Service at the University of East Anglia for access to the High Performance Computing Cluster.

**Keywords:** EPR spectroscopy • spin labels • Molecular Dynamics simulations • MTSL • protein dynamics

## References:

1. Berliner, L. J. 1989. Spin-labelling. Theory and Applications. Plenum Press.
2. Guo, Z., D. Cascio, K. Hideg, and W. L. Hubbell. 2008. Structural determinants of nitroxide motion in spin-labeled proteins: Solvent-exposed sites in helix B of T4 lysozyme. *Protein Sci.* 17:228-239.
3. Borbat, P. P., A. J. Costa-Filho, K. A. Earle, J. K. Moscicki, and J. H. Freed. 2001. Electron spin resonance in studies of membranes and proteins. *Science* 291:266-269.
4. Beier, C., and H.-J. Steinhoff. 2006. A structure-based simulation approach for electron paramagnetic resonance spectra using molecular and stochastic dynamics simulations. *Biophys. J.* 91:2647-2664.
5. Fanucci, G. E., and D. S. Cafiso. 2006. Recent advances and applications of site-directed spin labeling. *Curr. Opin. Struct. Biol.* 16:644-653.
6. Thompson, A. R., N. Naber, C. Wilson, R. Cooke, and D. D. Thomas. 2008. Structural Dynamics of the Actomyosin Complex Probed by a Bifunctional Spin Label that Cross-Links SH1 and SH2. *Biophys. J.* 95:5238-5246.
7. Freed, J. H. 2005. Biological Magnetic Resonance. In *Biomedical EPR – Part B: Methodology, Instrumentation, and Dynamics* G. Eaton, S. S. Eaton, and L. J. Berliner, editors. Kluwer, New York. 239-268.
8. Drescher, M., and G. Jeschke, editors. 2012. *EPR Spectroscopy Applications in Chemistry and Biology*. Springer.
9. Hubbell, W. L., A. Gross, R. Langen, and M. A. Lietzow. 1998. Recent advances in site-directed spin labeling of proteins. *Curr. Opin. Struct. Biol.* 8:649-656.
10. Nielsen, R. D., K. P. Che, M. H. Gelb, and B. H. Robinson. 2005. A ruler for determining the position of proteins in membranes. *J. Am. Chem. Soc.* 127:6430-6442.
11. Jeschke, G. 2013. Conformational dynamics and distribution of nitroxide spin labels. *Prog. Nucl. Magn. Reson. Spectrosc.* 72:42-60.
12. Columbus, L., T. Kalai, J. Jeko, K. Hideg, and W. L. Hubbell. 2001. Molecular motion of spin labeled side chains in alpha-helices: Analysis by variation of side chain structure. *Biochemistry* 40:3828-3846.
13. Kalai, T., M. Balog, J. Jeko, and K. Hideg. 1999. Synthesis and reactions of a symmetric paramagnetic pyrrolidine diene. *Synthesis-Stuttgart*:973-980.
14. Fleissner, M. R., E. M. Brustad, T. Kalai, C. Altenbach, D. Cascio, F. B. Peters, K. Hideg, S. Peucker, P. G. Schultz, and W. L. Hubbell. 2009. Site-directed spin labeling of a genetically encoded unnatural amino acid. *Proc. Natl. Acad. Sci. U.S.A.* 106:21637-21642.
15. Fawzi, N. L., M. R. Fleissner, N. J. Anthis, T. Kalai, K. Hideg, W. L. Hubbell, and G. M. Clore. 2011. A rigid disulfide-linked nitroxide side chain simplifies the quantitative analysis of PRE data. *J. Biomol. NMR* 51:105-114.
16. Fleissner, M. R., M. D. Bridges, E. K. Brooks, D. Cascio, T. Kalai, K. Hideg, and W. L. Hubbell. 2011. Structure and dynamics of a conformationally constrained nitroxide side chain and applications in EPR spectroscopy. *Proc. Natl. Acad. Sci. U.S.A.* 108:16241-16246.

17. Khramtsov, V. V., V. I. Yelinova, L. M. Weiner, T. A. Berezina, V. V. Martin, and L. B. Volodarsky. 1989. Quantitative-Determination of Sh-Groups in Low-Molecular-Weight and High-Molecular-Weight Compounds by an Electron-Spin Resonance Method. *Anal. Biochem.* 182:58-63.
18. Khramtsov, V. V., V. I. Yelinova, Y. I. Glazachev, V. A. Reznikov, and G. Zimmer. 1997. Quantitative determination and reversible modification of thiols using imidazolidine biradical disulfide label. *J. Biochem. Biophys. Methods* 35:115-128.
19. Weiner, L. M. 1995. Quantitative-Determination of Thiol-Groups in Low and High-Molecular-Weight Compounds by Electron-Paramagnetic-Resonance. *Method Enzymol* 251:87-105.
20. Hornak, V., R. Abel, A. Okur, B. Strockbine, A. Roitberg, and C. Simmerling. 2006. Comparison of multiple amber force fields and development of improved protein backbone parameters. *Proteins* 65:712-725.
21. Barone, V., A. Bencini, M. Cossi, A. Di Matteo, M. Mattesini, and F. Totti. 1998. Assessment of a combined QM/MM approach for the study of large nitroxide systems in vacuo and in condensed phases. *J. Am. Chem. Soc.* 120:7069-7078.
22. Stendardo, E., A. Pedone, P. Cimino, M. C. Menziani, O. Crescenzi, and V. Barone. 2010. Extension of the AMBER force-field for the study of large nitroxides in condensed phases: an ab initio parameterization. *PCCP* 12:11697-11709.
23. Frish M. J. , *e. a.* 2009. Gaussian 09 Revision C01, Gaussian Inc., Wallingford CT.
24. Autenrieth, F., E. Tajkhorshid, J. Baudry, and Z. Luthey-Schulten. 2004. Classical force field parameters for the heme prosthetic group of cytochrome c. *J. Comput. Chem.* 25:1613-1622.
25. Case, D. A., T. E. Cheatham, T. Darden, H. Gohlke, R. Luo, K. M. Merz, A. Onufriev, C. Simmerling, B. Wang, and R. J. Woods. 2005. The Amber biomolecular simulation programs. *J. Comput. Chem.* 26:1668-1688.
26. Oganessian, V. S. 2011. A general approach for prediction of motional EPR spectra from Molecular Dynamics (MD) simulations: application to spin labelled protein. *PCCP* 13:4724-4737.
27. Sezer, D., J. H. Freed, and B. Roux. 2008. Using Markov models to simulate electron spin resonance spectra from molecular dynamics trajectories. *J. Phys. Chem. B* 112:11014-11027.
28. DeSensi, S. C., D. P. Rangel, A. H. Beth, T. P. Lybrand, and E. J. Hustedt. 2008. Simulation of nitroxide electron paramagnetic resonance spectra from Brownian trajectories and molecular dynamics simulations. *Biophys. J.* 94:3798-3809.
29. Steinhoff, H. J., and W. L. Hubbell. 1996. Calculation of electron paramagnetic resonance spectra from Brownian dynamics trajectories: Application to nitroxide side chains in proteins. *Biophys. J.* 71:2201-2212.
30. Wolynes, P. G., and J. M. Deutch. 1977. Dynamical Orientation Correlations in Solution. *J. Chem. Phys.* 67:733-741.
31. Wang, D., U. Kreutzer, Y. R. Chung, and T. Jue. 1997. Myoglobin and hemoglobin rotational diffusion in the cell. *Biophys. J.* 73:2764-2770.
32. Kuprusevicius, E., G. White, and V. S. Oganessian. 2011. Prediction of nitroxide spin label EPR spectra from MD trajectories: application to myoglobin. *Faraday Discuss.* 148:283-298.
33. Buchete, N. V., and G. Hummer. 2008. Coarse master equations for peptide folding dynamics. *J. Phys. Chem. B* 112:6057-6069.
34. Tyrrell, S., and V. Oganessian. 2013. Simulation of electron paramagnetic resonance spectra of spin-labeled molecules from replica-exchange molecular dynamics. *Physical Review E* 88.

35. Springer, B. A., and S. G. Sligar. 1987. High-Level Expression of Sperm Whale Myoglobin in Escherichia-Coli. *Proceedings of the National Academy of Sciences of the United States of America* 84:8961-8965.
36. Brunori, E. A. a. M. 1971. Hemoglobin and myoglobin in their reactions with ligands. North-Holland: London and New York.
37. Karplus, M., and J. A. McCammon. 2002. Molecular dynamics simulations of biomolecules. *Nat. Struct. Biol.* 9:646-652.
38. Sezer, D., J. H. Freed, and B. Roux. 2009. Multifrequency Electron Spin Resonance Spectra of a Spin-Labeled Protein Calculated from Molecular Dynamics Simulations. *J. Am. Chem. Soc.* 131:2597-2605.
39. Oganessian, V. S. 2015. Computational approaches for simulating motional EPR spectra. In *SPR: Electron Paramagnetic Resonance*. B. C. Gilbert, V. Chechik, and D. M. Murphy, editors. Royal Society of Chemistry, London. 32-61.
40. Oganessian, V. S., E. Kuprusevicius, H. Gopee, A. N. Cammidge, and M. R. Wilson. 2009. Electron Paramagnetic Resonance Spectra Simulation Directly from Molecular Dynamics Trajectories of a Liquid Crystal with a Doped Paramagnetic Spin Probe. *Phys. Rev. Lett.* 102.
41. Chami, F., M. R. Wilson, and V. S. Oganessian. 2012. Molecular dynamics and EPR spectroscopic studies of 8CB liquid crystal. *Soft Matter* 8:6823-6833.
42. Phillips, S. E. 1980. Structure and refinement of oxymyoglobin at 1.6 Å resolution. *J Mol Biol* 142:531-554.
43. Arduengo, A. J., and E. M. Burgess. 1976. Structure of a Substituent Stabilized Thione Methylide. *J. Am. Chem. Soc.* 98:5021-5023.
44. Sezer, D., J. H. Freed, and B. Roux. 2008. Parametrization, molecular dynamics simulation, and calculation of electron spin resonance spectra of a nitroxide spin label on a polyalanine alpha-helix. *J. Phys. Chem. B* 112:5755-5767.

**Highlights**

EPR measurements and fully atomistic Molecular Dynamics (MD) simulations provide evidence for intrinsic low rotameric mobility of Rn nitroxyl spin label. This study uncovers the potential of using Rn spin label as a reporter of protein motions.

ACCEPTED MANUSCRIPT